# Effect of heat transfer through the release pipe on simulations of cryogenic hydrogen jet fires and hazard distances

[1*]*Donatella Cirrone*, [1]*Dmitriy Makarov*, [2]*Mike Kuznetsov*, [3]*Andreas Friedrich*, [1]*Vladimir Molkov*
[1]*HySAFER Centre, Ulster University, Newtownabbey, Northern Ireland, BT37 0QB, UK*
[2]*Karlsruhe Institute of Technology, 76131, Karlsruhe, Germany*
[3]*Pro-Science, 76725, Ettlingen, Germany*

## Abstract

Jet flames originated by cryo-compressed ignited hydrogen releases can cause life-threatening conditions in their surroundings. Validated models are needed to accurately predict thermal hazards from a jet fire. Numerical simulations of cryogenic hydrogen flow in the release pipe are performed to assess the effect of heat transfer through the pipe walls on jet parameters. Notional nozzle exit diameter is calculated based on the simulated real nozzle parameters and used in CFD simulations as a boundary condition to model jet fires. The CFD model was previously validated against experiments with vertical cryogenic hydrogen jet fires with release pressures up to 0.5 MPa (abs), release diameter 1.25 mm and temperatures as low as 50 K. This study validates the CFD model in a wider domain of experimental release conditions - horizontal cryogenic jets at exhaust pipe temperature 80 K, pressure up to 2 MPa abs and release diameters up to 4 mm. Simulation results are compared against such experimentally measured parameters as hydrogen mass flow rate, flame length and radiative heat flux at different locations from the jet fire. The CFD model reproduces experiments with reasonable for engineering applications accuracy. Jet fire hazard distances established using three different criteria - temperature, thermal radiation and thermal dose - are compared and discussed based on CFD simulation results.

**Keywords**: cryogenic hydrogen, jet fires, conjugate heat transfer, radiative heat transfer, hazard distances

## 1. Introduction

Cryo-compression of hydrogen gas is a competitive technique to store and transport large quantities of hydrogen, due to higher gravimetric and volumetric capacities than compressed gas at ambient temperature [1]. The increasing deployment of such hydrogen applications requires a deep understanding of the consequences resulting from potential accidents with a cryogenic release. This knowledge is of furthermost importance to protect life and prevent property loss for an inherently safer hydrogen infrastructure. In case of an unintended release from equipment or Thermally activated Pressure Relief Device (TPRD) opening, hydrogen can be ignited producing a jet fire. The thermal hazards from cryogenic hydrogen jet fires were mainly experimentally investigated. Authors in [2] analysed the thermal radiation emitted by hydrogen ignited releases with absolute pressures up to 3.5 MPa and temperature in the range 34-65 K. A maximum radiation level as high as 10 kW/m$^2$ was recorded at 0.75 m from the jet axis, which is sufficient to provoke second-degree burns after 20 s exposure according to published harm criteria [3]. Sandia National Laboratories (SNL) performed experiments on cryogenic jet fires with release temperature down to 37 K and pressures up to 0.6 MPa abs [4]. Experimental measurements showed an increase of radiative heat flux for decreasing release temperature at a given mass flow rate. Previous work by the authors validated a computational fluid dynamics (CFD) model to simulate flame length and radiative heat flux for cryogenic hydrogen jet fires against SNL experiments on jet fires from cryogenic hydrogen storage with pressure up to 0.5 MPa abs and temperature in the range 48-82 K [5].

The heat transfer through the wall of a release pipe connecting the storage system to the nozzle affects the cryogenic flow characteristics. The first part of the present study aims at numerical simulations of the cryogenic hydrogen flow through the portion of a release pipe exposed at the external surface to ambient temperature to assess the effect of conjugate heat transfer on the flow parameters in the real nozzle. The study will then analyse the capability of a notional nozzle theory applied to cryogenic under-expanded jets by using the parameters obtained at the real nozzle exit by the CFD simulations. The notional nozzle parameters are implemented then as an input into the CFD simulations of hydrogen jet fires. The CFD model previously developed and validated against vertical hydrogen jet fires with release pressure up to 0.5 MPa abs is employed to expand its range of applicability, i.e. the validation

domain, to horizontal jet fires with higher storage pressure and larger nozzle diameter [5]. The experiments were performed at Karlsruhe Institute of Technology (KIT) on ignited hydrogen releases at the temperature 80 K and pressures 0.3-2.0 MPa. The capability of the CFD model to predict accurately experiments is assessed through comparison with experimentally measured in several locations radiative heat flux and the flame length.

One of goals of this study is the calculation of hazard distances from the cryogenic jet fires. Predictive engineering tools are available in the literature to calculate hazard distances from the momentum-dominated hydrogen jet fires using the flame length correlation and available in literature temperature distribution along jet fire axis [6]. The "fatality" limit condition is achieved at a distance ($x$) equal to the twofold flame length ($x = 2L_f$), the "pain" limit at $x$=3$L_f$ and the "no harm" limit at $x$=3.5$L_f$. In horizontal jet fires, combustion products will raise up because of the buoyancy. This may lead to reduction of hazard distances along the original jet axis. The thermal dose is well suited for estimating thermal hazards from a jet fire, as it takes into account both the exposure duration and the radiative heat flux. Only a few studies employed the thermal dose as a parameter to define hazard levels from a cryogenic hydrogen jet fire. Experimental work [7] on jet fires from a 60 l/min liquid hydrogen ($LH_2$) release calculated the thermal dose from radiative heat flux measured at 7.6 m and 8.7 m along the jet axis. The authors concluded that distance greater than 8.7 m from the jet fire, which had an extent of 5 m, should be maintained to avoid a harmful thermal dose of 92 $(kW/m^2)^{4/3}s$ for an exposure time up to 200 s. A time of 28 s was found to be sufficient to reach the pain limit at 7.6 m under wind conditions (2.15 m/s), whereas a longer exposure time of 44 s was needed in lower wind conditions (0.59 m/s). In both cases direction of wind was South-West, whereas that of the release was North-East [7]. The computational study [8] calculated the thermal dose levels in the vicinity of cryogenic jet fires with release temperature in the range 48-78 K and storage pressure 0.2-0.4 MPa abs from 1.25 mm orifice. It was concluded that for all tests, at 0.5 m from the flame axis people should stand less than 30 s to not incur in first degree burns.

The present study aims at further enhancement and validation of the CFD model accounting for the effect of heat transfer in the release pipe on flow parameters and assessing thermal hazard distances for horizontal cryogenic jet fires with release pressure and diameter up to 2 MPa and 4 mm respectively. The analysis is focused on distributions of temperature, thermal radiation and thermal dose along and aside of the jet axis. As mentioned above, the horizontal jet fire and combustion products may be affected by buoyancy, causing the tilting of the flame axis. For this reason, the study distinguishes the release direction from the flame tilted axis.

## 2. Description of validation experiments

Experiments on cryogenic hydrogen jet fires were performed at the ICESAFE facility of Karlsruhe Institute of Technology (KIT) in Germany [9]. Hydrogen was released horizontally at a height of 0.9 m inside a 160 $m^3$ chamber with dimensions 8.5x3.4x5.5 m. The facility was designed for quasi-steady-state release conditions, with constant release temperature and pressure. The mass flow rate is measured using a Coriolis mass flow meter (Micro Motion CMF010) with an accuracy of ±0.35%. Figure 1a shows a schematic of the release system used in the experiments. Hydrogen flow temperature and pressure were measured at the location marked as "cross". Hydrogen conditions readings at the "cross" are taken as representative of hydrogen storage conditions. Afterwards, the gas flows in a pipe of unknown length, then through a valve and finally in a 60 mm pipe before the discharge into the atmosphere. The pipe has the inner diameter equal to 10 mm and the outer diameter 12 mm. The geometry and dimensions of the pipe are shown in Fig. 1b. The nozzle is located on the right-hand side of the pipe. Overall, six tests were performed for different temperature, pressures and release diameters. Table 1 shows the operating conditions for six experiments. The nozzle diameter is *D*=2 mm for Tests 1, 3 and 4, and *D*=4 mm for Tests 2, 5 and 6. Two tests series were performed for hydrogen at ambient temperature (290 K). Four tests were performed with cryogenic hydrogen (80 K). For cryogenic releases, hydrogen underwent a cooling-down procedure by flowing in a LN2 bath at 77 K after measurement of the mass flow rate through the Coriolis mass flow meter. During the pre-cooling process, which took approximately 1 hour, the hydrogen flow was bypassed and redirected to the cooling system. Both ambient temperature and cryogenic tests will be used to analyse the release source

modelling capabilities. The CFD modelling of jet fires will be focused on the four tests with hydrogen at cryogenic temperature, as it is the main objective of the study.

The jet was ignited after 2 s of the release to establish the steadiness of the process. Ignition was triggered at 0.4 m from the release point and had a duration of 400 ms. The jet flame duration was 8 s to reach a saturation of the radiative heat flux at the sensors. Two different sensors were available and were located as a pair at each given position. The sensors have the following characteristics:

- One sensor had no window with optical filter and recorded the full spectrum of incident radiation. This sensor measurement will be indicated as NW.
- Another sensor had a ZnSe filter in window to record the incident radiation with wavelengths in the range 0.5-22 µm, which includes the range 2-9 µm for steam radiation. This sensor will be indicated as ZnSeW.

In the tests the sensors were located at the same height as the jet fire (0.9 m) and were moved in nine steps of 0.25 m distance on a movable support parallel to the release direction. For each position a separate test with exactly the same release conditions was performed. In the first series the support was located at distance 0.5 m from the release direction, in two further test series the sensors support was moved to 0.75 m and then 1.25 m from the jet axis to permit measurements with increasing distance from the jet fire. Figure 1c shows the location of radiometers with respect to the jet flame and reports the univocal denomination for each sensor configuration (every symbol corresponds to one experiment with both sensors in the respective position).

The flame length ($L_f$) was experimentally determined as $\frac{X_{Q,max}}{0.6}$, where $X_{Q,max}$ is the distance at which the maximum radiative heat flux was recorded. This consideration is consistent with observations on the distance along the jet axis where the highest temperature is recorded: $X_{T,max} = 0.6L_f$ [10].

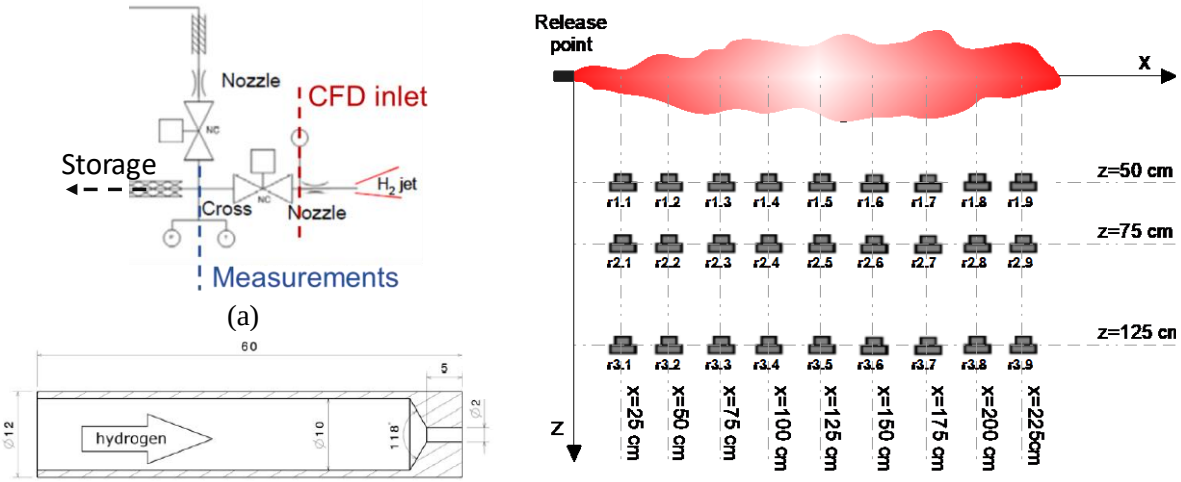


*Figure 1. a) experimental release system; b) drawing of the pipe section with nozzle on the right-hand side, all dimensions in mm; c) top view of the experimental set-up for thermal radiation measurements at height 0.9 m [9].*

## 3. Release source modelling

Table 1 shows that experimental bulk pressures were in the range 0.3-2 MPa abs. Thus, jets were under-expanded with pressure at the real nozzle exit being higher than atmospheric. The expansion of the flow to ambient pressure is characterised by shock waves and supersonic velocities. An accurate resolution of the expansion zone in simulations requires higher refinement and complex numerical codes. The alternative and widely used methodology is applied. The notional nozzle theory is employed to model the release sources in the jet fires simulations [6, 11]. The flow at the notional nozzle exit has expanded to ambient pressure and has a uniform sonic velocity that allows the use of faster incompressible codes.

### 3.1 Notional nozzle approach

The under-expanded jet theory [11] showed to represent well cryogenic hydrogen releases with the temperature down to 46 K and pressure up to 0.6 MPa ([5,12]). This theory uses Abel-Noble Equation

of State (EOS) to account for the non-ideal behaviour of hydrogen gas at high pressure. The theory assumes an isentropic expansion from the stagnation pressure in a storage vessel through the real nozzle and, finally, after the jet expansion to the atmospheric pressure through the notional nozzle exit. The equations for energy and mass conservation are employed in an assumption of a sonic flow to calculate conditions at the notional nozzle exit. Firstly, it was verified that pressure measured at the "cross" (Fig. 1a) can be assumed as stagnation condition, given the non-zero velocity in the pipe. It was estimated that the associated dynamic pressure is less than 0.04% of the static pressure, confirming that it can be neglected, and stagnation assumption be used. Table 1 shows the directly calculated notional nozzle exit parameters and mass flow rate assuming adiabatic (no heat exchange) flow conditions. It can be observed that the mass flow rate for warmer releases is reasonably predicted within ±15% accuracy. On the other hand, the mass flow rate for cryogenic releases is significantly overestimated up to 37% for Test 4. A discharge coefficient, $C_D$, can be introduced in calculations to match the experimental flow rate. In the general case, its value is affected by friction and minor losses in release path and possible non-zero velocity of the gas in the storage vessel. The discharge coefficient is a dimensionless number and was defined (see Table 1) through the inverse problem method by exact matching of the experimental mass flow rate: $\dot{m}_{exp} = C_D \cdot \rho \cdot u \cdot A$. Table 1 presents the calculated notional nozzle parameters applying the discharge coefficient. It can be seen that Test 3 ($D$=2mm) and Test 5 ($D$=4mm) would result in the same notional nozzle characteristics to be imposed in CFD simulations, and hence in the same jet fires. Similar observations can be done for Test 4 ($D$=2mm) and Test 6 ($D$=4mm). However, experiments demonstrated that the larger release diameter results in the higher radiative heat flux and the longer flame lengths. Thus, it can be concluded that the simple application of the discharge coefficient to match the experimental mass flow rate is not sufficient to correctly simulate a cryogenic release, as not capable to catch the variation in release conditions due to the presence of heat transfer even if the mass flow rate could be met exactly. Therefore, a different approach is used.

*Table 1. Experimental conditions of the validation tests* [9]. *Pressure and temperature are measured at the "cross" upstream a valve and 60 mm release pipe (see release system in Fig. 1a). Notional nozzle exit parameters.*

| **Test No.** | **1** | **2** | **3** | **4** | **5** | **6** |
|---|---|---|---|---|---|---|
| *Experimental operating conditions* | | | | | | |
| Pressure, MPa abs | 2.0 | 0.4 | 1.4 | 2.0 | 0.3 | 0.4 |
| Temperature, K | 290 | 290 | 80 | 80 | 80 | 80 |
| Real nozzle diameter, mm | 2 | 4 | 2 | 2 | 4 | 4 |
| Experimental mass flow rate, g/s | 3.3 | 3.3 | 3.3 | 4.4 | 3.3 | 4.4 |
| *Notional nozzle exit parameters* | | | | | | |
| Temperature, K | 241.7 | 241.7 | 66.7 | 66.7 | 66.7 | 66.7 |
| Velocity, m/s | 1181.3 | 1181.3 | 620.4 | 620.4 | 620.4 | 620.4 |
| Density, kg/m$^3$ | 0.102 | 0.102 | 0.369 | 0.369 | 0.369 | 0.369 |
| *Calculations without a discharge coefficient $C_D$* | | | | | | |
| Notional nozzle diameter, mm | 6.43 | 5.77 | 5.35 | 6.36 | 4.99 | 5.76 |
| Calculated mass flow rate, g/s | 3.90 | 3.14 | 5.13 | 7.27 | 4.47 | 5.95 |
| Deviation of calculated mass flow rate from experiment, % | 15.4 | -5.1 | 35.7 | 37.3 | 26.2 | 26.0 |
| *Calculations with the inclusion of a discharge coefficient $C_D$* | | | | | | |
| Defined discharge coefficient | 0.85 | 1.00 | 0.64 | 0.60 | 0.74 | 0.74 |
| Notional nozzle diameter, mm | 5.93 | 5.77 | 4.3 | 4.93 | 4.3 | 4.96 |
| Calculated mass flow rate, g/s | 3.3 | 3.14 | 3.3 | 4.4 | 3.3 | 4.4 |

### 3.2 Numerical simulations of cryogenic hydrogen flow in the release pipe

Applying a discharge coefficient is limited to the characterisation of the flow based on pressure losses in the release system. Instead, CFD simulations are performed to characterise hydrogen flow parameters accounting for heat transfer between the cryogenic flow and the pipe wall. Hydrogen conditions measured at the "cross" are taken as the inlet boundary conditions in the CFD simulations of hydrogen flow in the 60 mm pipe (see Fig. 1a) with geometry and dimensions as shown in Fig. 1b.

*3.2.1. The CFD model and numerical details*

The CFD model uses an LES explicit density-based solver. The dynamic Smagorinsky-Lilly sub-grid scale model is applied for turbulence [13]. The time step is dictated by a Courant-Friedrichs-Lewy number equal to CFL=0.9. The specific heat of hydrogen is defined as a polynomial function interpolating NIST data for cryogenic temperatures [14]. Simulations are performed in a cylindrical domain with radius 70 mm and axial length 180 mm (three times the tube length). The release nozzle is discretized with 13 cells along the diameter, as suggested in [15], leading to an average cell size dimension of 0.15 mm for the 2 mm nozzle. The total number of control volumes (CV) is 263,110. The solid pipe walls are included in the numerical grid to model the conjugate heat transfer through them. The inner and outer walls are defined as coupled, which means that the heat transfer is calculated directly from the solution in the two cells adjacent to the wall, respectively in the fluid and solid zones. The wall is discretized with 19 cells in radial direction from the inner to the outer wall. The cell size varies with a growing ratio of 1.1 from 34 μm to 62 μm in the pipe section with thickness 1 mm. Steel properties are defined as 8030 kg/m$^3$ for density, 502.48 J/kg/K for specific heat and 16.27 W/m/K for thermal conductivity [16]. The details of the release pipe geometry and a "zoom in" of the numerical grid of the pipe near field are shown in Fig. 2. A pressure inlet condition is imposed at the pipe entrance. Inlet pressure and temperature are defined as in Table 1. The boundaries of the domain are defined as pressure outlet with gauge pressure equal to 0. The air composition is taken as 0.21 of oxygen ($O_2$) and 0.79 of nitrogen ($N_2$) by mole fraction. The temperature of 288 K is imposed at the external boundaries and as initial conditions for air temperature. The second-order upwind scheme is used for the flow spatial discretization along with least square cell-based for gradients.

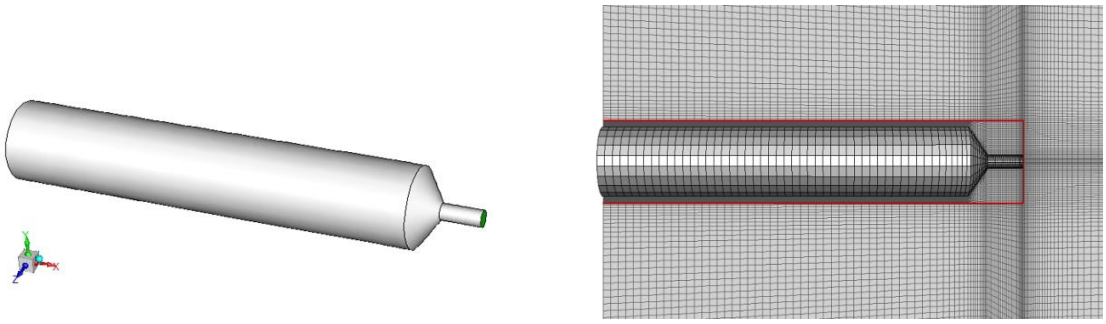

(a) (b)

*Figure 2. Geometry and mesh: a) geometry of the internal walls of the release pipe; b) the numerical grid of the pipe internal walls, the outline of the pipe external walls (red solid lines) and "zoom in" of the numerical grid in the near field.*

*3.2.2. Results and discussion*

A first assessment of the effect of heat transfer through the pipe walls is conducted for Test 3. Figure 3a shows a comparison of mass flow rate at the real nozzle exit for adiabatic and non-adiabatic pipe walls. The hydrogen flow stabilises during 2-7 ms, as confirmed by the constant flow beyond this time. Figure 3b shows the radial distribution of temperature at an axial distance of 50 mm, i.e. in the ending section of the pipe with the inner diameter 10 mm for the time 12 ms. It can be observed that temperature at the axis is the same for both the cases, however, radially, the inclusion of heat transfer causes an increase of temperature of the fluid towards the wall at 5 mm radial distance, reaching almost 150 K in the layer of cells closer to the wall. Similarly, the temperature at the nozzle exit is not uniformly distributed (see Fig. 4). The temperature in the core of the flow is approximately 57 K and it rapidly increases towards the tube walls up to 105 K due to heat transfer. Therefore, the temperature averaged by the nozzle cross area is considered in this case (71.4 K). This value was compared with the average calculated by weighting temperature by mass (68.2 K). Variation resulted to be within 5%. Variation of temperature increased up to 8% when compared to the average weighted by enthalpy (65.6 K). It is considered that this variation is negligible compared to the overestimation of experimental mass flow rate by the notional nozzle approach not including effect of heat transfer (37.3%). Thus, the parameters at the nozzle averaged by the nozzle cross area will be considered throughout the following text. When the heat transfer through the walls is included in simulations (non-adiabatic walls), the calculated established mass flow rate is 4.25 g/s and the temperature of hydrogen at the nozzle exit is 71.4 K. The heat transfer rate through the wall is equal to 754 W, 75% of which goes through the pipe of wider

diameter 10 mm. If the heat transfer through the wall is not included, the hydrogen mass flow rate is approximately 9% higher (4.65 g/s) and the temperature of the flow is lower (56 K).

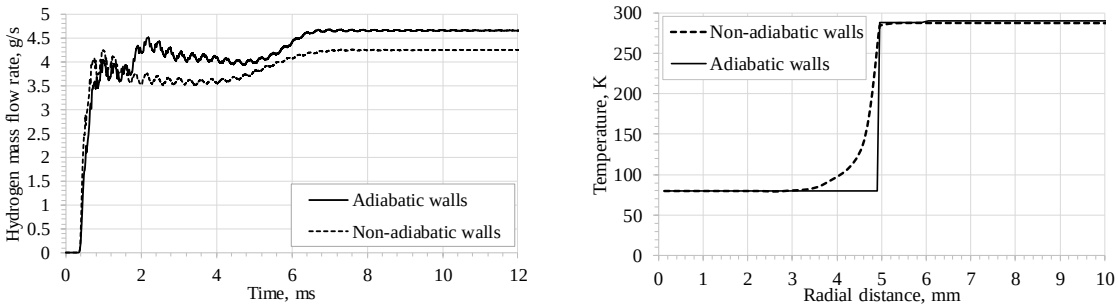


(a) (b)

*Figure 3. Effect of heat transfer through the pipe walls (non-adiabatic vs adiabatic walls) for Test 3: (a) hydrogen mass flow rate; (b) temperature radial distribution at 50 mm axial distance at 12 ms.*

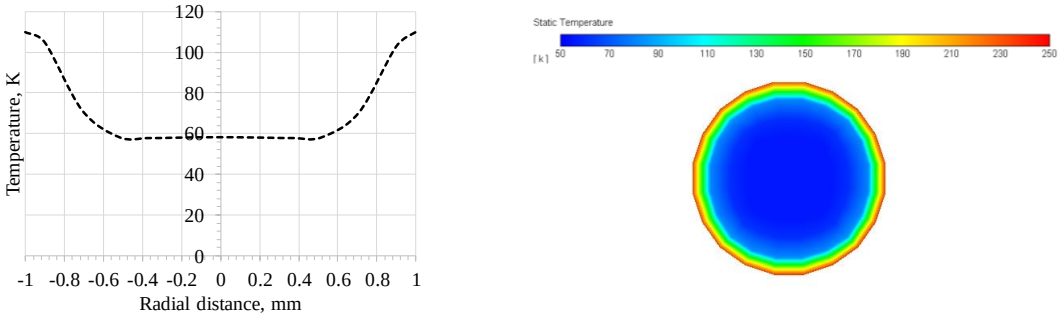


(a) (b)

*Figure 4. Distribution of temperature at the real nozzle exit at 12 ms: non-adiabatic pipe walls simulation for Test 3.*

A mesh sensitivity analysis is performed by halving the cell size in the zone (12x120 mm) that includes the release pipe and surrounding near zone. The resulting mesh has 943,265 CVs. The mesh refinement causes an increase by 7.6% of the integral heat flux through the pipe walls for Test 3. The maximum relative difference in the calculated mass flow rate is 3.8%, whereas it is negligible for the other parameters at the nozzle, e.g. temperature. Thus, it is concluded that the level of accuracy of the solution is acceptable compared to the gain in computational time required by calculations.

Simulations are performed for the remaining three tests with hydrogen at cryogenic temperature by changing the inlet pressure and numerical grid for the respective release nozzle. Table 2 shows the resulting flow parameters at the real nozzle exit cross-section. Generally, it can be observed that the discrepancy between simulated and experimentally measured mass flow rates increases with the inlet pressure, reaching almost 30% for Test 4 at the highest inlet pressure (2.0 MPa). As shown in Table 2, higher pressures are associated with larger heat transfer in the 60 mm pipe, due to a higher velocity of the flow and thus higher convective heat transfer between hydrogen and the pipe. As shown in Fig. 1a, the hydrogen temperature and pressure (hereby considered as inlet conditions for the CFD simulations) were measured somewhere upstream the simulated release pipe. From the measurement location to the actual inlet of the 60 mm pipe, the cryogenic hydrogen gas flows in a pipe of unknown length and through a valve. The authors believe that the cause of the discrepancy in the calculated mass flow rate is to be looked for in the heat transfer taking place in the release system between the measurement location and the 60 mm pipe.

*Table 2. Parameters at the real nozzle calculated from CFD modelling including conjugate heat transfer through the 60 mm pipe walls.*

| **Test No.** | | **3** | **4** | **5** | **6** |
|---|---|---|---|---|---|
| Inlet | Temperature, K | 80 | 80 | 80 | 80 |
| | Pressure, MPa | 1.4 | 2 | 0.3 | 0.4 |
| | Diameter, mm | 2 | 2 | 4 | 4 |
| | Temperature, K | 71.4 | 70.7 | 75.9 | 73.3 |

| | | | | | |
|---|---|---|---|---|---|
| Real nozzle exit | Pressure, MPa | 0.499 | 0.705 | 0.122 | 0.160 |
| | Velocity, m/s | 798.7 | 801.2 | 746.1 | 750.9 |
| | Density, kg/m$^3$ | 1.798 | 2.566 | 0.423 | 0.570 |
| | Calculated mass flow rate, g/s | 4.25 | 6.10 | 3.88 | 5.2 |
| | Variation of calculated mass flow rate from experiment, % | 22.4 | 27.8 | 15.0 | 15.4 |
| Pipe wall | Total surface heat flux, W | 754.4 | 973.2 | 680.0 | 794.9 |

*3.2.3. Adjustment of inlet conditions*

In this section, the inlet temperature is modified to include the effect of heat transfer in the release system upstream of the 60 mm release pipe ending with the real nozzle. Inlet temperature has been gradually increased by +10 K value until the best fit with the experimental mass flow rate is found. Table 3 shows the resulting parameters at the real nozzle exit. This is considered to be a rational procedure to estimate the flow characteristics, as it was shown that the inclusion of heat transfer in just 60 mm pipe for Test 3 is capable to cause an increase of temperature by 16 K at the real nozzle exit. A longer pipe, as present between the sensor location and the nozzle, may result in a larger temperature difference. As expected, releases at higher pressure result in a higher inlet temperature because of the expected higher heat flux.

*Table 3. Parameters at the real nozzle exit calculated from CFD simulations including conjugate heat transfer through the pipe walls and inlet temperature modification. Calculated notional nozzle exit parameters accounting for the effect of conjugate heat transfer in the 60 mm release pipe and hydrogen path downstream to the location "cross" where measurements of temperature and pressure were performed.*

| **Test No.** | | **3** | **4** | **5** | **6** |
|---|---|---|---|---|---|
| Inlet | Temperature, K | 140 | 150 | 110 | 110 |
| | Pressure, MPa | 1.4 | 2 | 0.3 | 0.4 |
| Real nozzle exit | Diameter, mm | 2 | 2 | 4 | 4 |
| | Temperature, K | 120.7 | 126.7 | 100.0 | 98.4 |
| | Pressure, MPa | 0.549 | 0.788 | 0.127 | 0.168 |
| | Velocity, m/s | 967.5 | 989.2 | 835.9 | 844.7 |
| | Density, kg/m$^3$ | 1.12 | 1.52 | 0.322 | 0.43 |
| | Calculated mass flow rate, g/s | 3.28 | 4.55 | 3.34 | 4.47 |
| | Variation of calculated mass flow rate from experiment, % | -0.6 | 3.6 | 1.2 | 1.6 |
| Notional nozzle exit | Temperature, K | 120.6 | 126.8 | 99.4 | 97.7 |
| | Velocity, m/s | 834.4 | 855.6 | 757.4 | 751.0 |
| | Density, kg/m$^3$ | 0.204 | 0.194 | 0.247 | 0.252 |
| | Diameter, mm | 5.0 | 6.0 | 4.8 | 5.6 |

The CFD simulations of the hydrogen flow in the release pipe allow calculating the flow characteristics at the real nozzle exit taking into account the effect of conjugate heat transfer through the release pipe. The simulated parameters are used to estimate the flow characteristics at the notional nozzle exit where the gas has fully expanded to ambient pressure. The flow is assumed to expand isentropically between the real nozzle and the notional nozzle exits. The equations for mass and energy conservation, along with the assumption of uniformly sonic speed, are used to estimate parameters at the notional nozzle exit, including its diameter. Table 3 shows the calculation results that will be used as inlet conditions in numerical simulations of the hydrogen jet fires.

## 4. Jet fire modelling

### 4.1. The CFD model of hydrogen jet fire

The CFD model employed here was previously validated against vertical cryogenic hydrogen jet fires and is described in our paper [5]. ANSYS Fluent is used as a software platform. Numerical simulations employ a pressure-based solver and so called "incompressible ideal gas" assumption for the flow (i.e. density calculation based on constant pressure and variable temperature). A Reynolds-Averaged Navier-Stokes (RANS) approach is used to resolve conservation equations for mass, momentum, energy

and species. A turbulent Schmidt number, $Sc_t$, equal to 0.9, is used in the governing equations. Realizable k-ε model of turbulence is applied [17], by solving the transport equations for turbulence kinetic energy, $k$, and turbulent dissipation rate, $\varepsilon$. Combustion is modelled through the Eddy Dissipation Concept (EDC) model [18]. The CFD model includes detailed chemical mechanisms for hydrogen combustion in air through 18 elementary reactions and 9 species. Details of the chemical reaction mechanism are described in [19]. Radiation is modelled through the Discrete Ordinates (DO) model [20]. A refinement of 10x10 rays and 3x3 pixels is employed for discretising the radiative transfer equation (RTE), as suggested in [5] following sensitivity analysis. For hydrogen combustion in air, the only emitting and absorbing specie is water vapour, hereby considered as a grey gas. A function of Planck mean absorption coefficient on temperature and $H_2O$ partial pressure interpolating Hubbard and Tien's data available in [21] is used in the study. Simulations are steady-state, given that they aim at modelling established jet fires with constant release conditions. Convective terms in governing equations are discretised with a second-order upwind scheme, whereas a SIMPLE approach is used for velocity-pressure coupling.

### 4.2 Computational domain and numerical details

A domain with the same size as the test chamber (8.5x3.4x5.5m) is considered. The overall domain counts 1,322,921 CVs. Numerical grid is hexahedral. Figure 5a shows the numerical grid on plane in the vertical cross section at z=0, parallel to the hydrogen jet direction. The release pipe is assumed to have a length equal to 10 cm and the same cross-section as the notional nozzle exit. The release source is located at a distance of 0.5 m from the domain boundary behind it. The release source is modelled as one square cell with an area equivalent to that of the round notional nozzle exit (see diameter in Table 3). Thus, minimum cell size in the numerical grid is the length of the square release for each test, e.g. 4.5 mm for Test 3. A maximum cell growth ratio of 1.1 is set in proximity of the jet fire. The details of the numerical grid in the proximity of the release point are shown in Fig. 5b. Radiometers are modelled as 2x2 cm square surfaces, located as in the experiments (see Fig. 1c). The cell size in the jet fire zone and between the radiometers is maintained equal to 2 cm. The lateral and top external boundaries of the domain are modelled as pressure outlet with gauge pressure equal to 0. The choice to model the chamber lateral walls as open boundaries was dictated by the choice of steady-state simulations. The floor is defined as an adiabatic wall with emissivity 0.6, as indicated for steel in [22]. The notional nozzle exit is modelled as a velocity inlet, with parameters as defined in Table 3. A turbulent intensity of 25% and turbulent length scale equal to $0.07D_{not}$ are set at the inlet, following conclusions of the study [5]. Radiometers are modelled as non-slip and isothermal surfaces with emissivity 1, to prevent radiation reflection and to take into account the entire incident radiation. As the initial conditions the temperature was equal to 288 K and relative humidity equal to 77%, which is the average annual value recorded in the location of experiments [23]. These conditions are set for the entraining air at the external boundaries. Simulations are performed as well for a relative humidity of 50%, which is the parameter generally suggested for controlled environments, such as laboratories and testing facilities.

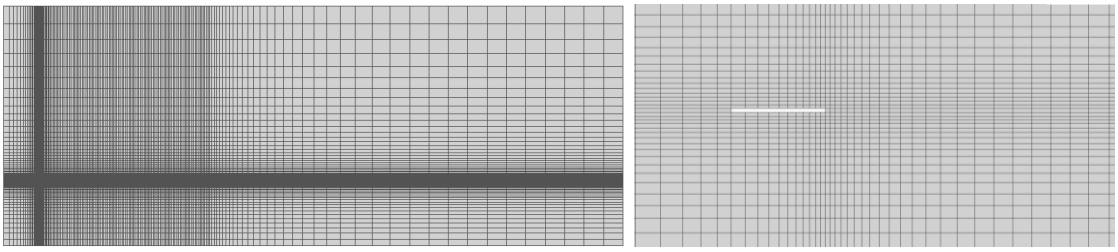

(a) (b)

*Figure 5. a) view of the numerical grid in plane z=0; b) zoomed-in view of the numerical grid close to the release.*

#### *4.2.1 Preliminary assessment on simulation procedure to accelerate calculations*

Simulations with the current DO discretisation (10x10 rays) and the number of CVs over 1 million may require a significant amount of simulation time. Thus, a preliminary assessment of the simulation details and procedures was performed, to reduce the simulation time while maintaining an acceptable accuracy level. The preliminary assessment was conducted on simulations for vertical cryogenic hydrogen jet fires previously validated against SNL experiments [5], given the smaller domain size and number of

CVs requiring a lower calculation time. The converged distributions of temperature and combustion products, and the radiative heat flux at sensors were monitored to assess the effect of the modifications.

The first analysis was conducted on the chemistry detail level. The number of reactions involved in combustion was reduced to 1 and the number of species to 4. An increase of recorded radiative heat flux up to 10% was observed at sensors located closer to the release point, due to the higher water vapour mole fraction along the jet axis when considering 1 reaction, instead of more species, e.g. 18 reactions and 9 species scheme, populating the combustion products. The effect was progressively reduced towards the tip of the jet fire. Reduction of the calculation time was only 30%, which is not considered sufficient to justify the consequent loss of accuracy. Thus, a chemistry detail level of 18 reactions and 9 species was maintained for the following simulations. Simulations are steady-state and chemistry is updated at every iteration of the flow. The jet fire distribution of reacting species and temperature is considered to be largely dominated by the momentum of the jet. The number of iterations per chemistry update was progressively increased to 2 and then to 5. The time required to reach a converged solution was reduced by about 15% when updating chemistry every 2 flow iterations, and by over a factor of 2 when this value was increased to 5. In both cases the maximum variation of radiative heat flux sensed at sensors was 2%. Thus, 5 iterations per chemistry update were chosen for the subsequent simulations, as variation in radiative heat flux was deemed to be negligible compared to the significant gain in calculation time. The RTE solved through the DO model is generally updated every 10 flow iterations. This number was increased to 100 and 200, and the variation on the resulting radiative heat flux at sensors was within 0.1%. However, the calculation time was reduced by a factor of 3 for 200 iterations. Based on the conclusions drawn for SNL jet fires, simulations in the present study implement a chemistry and DO model update every 5 and 200 flow iterations, respectively.

### 4.3 Results and discussion

Simulations of jet fires are performed for all four tests on cryogenic releases. CFD simulations allow gaining insights into the established distribution of temperature and combustion products in a jet fire. Comparison with experiments is performed for the radiative heat flux measured at the sensors and the jet fire flame length. Figure 6a shows the resulting distribution of temperature, water vapour and hydroxyl (OH) mole fraction in the entire domain for Test 3. It can be observed that distributions of temperature and water vapour are affected by buoyancy which can qualitatively lead to a decrease of hazard distance defined by thermal hazards from the jet fire. The OH mole fraction distribution gives insights into the zone of the jet fire mainly involved in the combustion reaction.

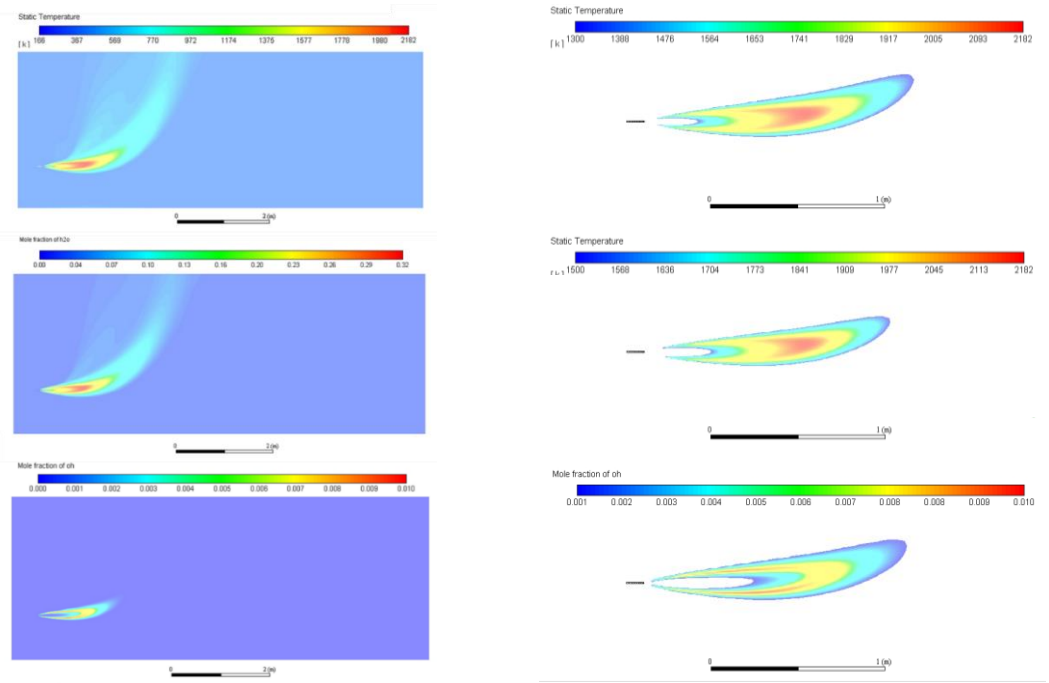


(a) (b)

*Figure 6. a) distribution of temperature, H2O and OH mole fraction in plane z=0 for Test 3; b) flame length visualization for Test 3 simulation using the following criteria (from top to bottom): temperature threshold 1300K, temperature threshold 1500K, hydroxyl mole fraction threshold 0.001.*

Figure 7 shows the calculated radiative heat flux for relative humidity (Rh) 77% and 50% versus experimental measurements at sensors for Tests 3 and 4 (*D*=2 mm). Experimental records by both of the two radiometers typologies, i.e. through NW and ZnSeW windows, are reported for comparison. Diamonds for each curve represent the records at 9 sensors located on the same line parallel to the release direction and shown in Fig. 1c. Test 3 simulation for Rh=77%, i.e. the yearly average for the facility location, reproduces experimental radiative heat flux at sensors at 50 cm and 75 cm from the axis with an accuracy of 10%. The exception is given by sensors r1.5, r1.7 and r1.9, where a maximum variation of +25% is reached in the simulations. However, simulation results underestimate experiments for the line of sensors at z=125 cm (r3.1-3.9), reaching a maximum variation of 30% towards the central zone of the jet fire. Similar observations can be made for Test 4. Radiative heat flux is predicted with an accuracy within 20% for the sensors located at distances 50 and 75 cm from the jet axis (r1.1-r1.9, r2.1-r2.9). On the other hand, simulation presents an underestimation up to 40% for the sensors at a distance of 125 cm from the axis (r3.1-r3.9). Several tests were performed ensuring same release pressure and temperature to measure the radiative heat flux at different distances from the jet by moving the sensors' support. Therefore, a possible decrease of pressure in between tests due to the storage tank blowdown may be excluded from the possible causes of underestimation of simulated radiative heat flux at 1.25 m distance. Figure 7 includes results of simulated radiative heat flux for a relative humidity equal to 50%. The relative difference between cases with Rh=50% and 77% increases with distance from the jet axis, varying from 16% for the sensors r1.1-r1.9 at 50 cm from the jet to 27% for sensors r3.1-r3.9 at z=125 cm. For both Tests 3 and 4, simulated radiative heat flux with Rh=50% overlaps with experiments at the furthest distance from the jet axis, conversely to the underestimation observed with Rh=77%. It is believed that actual relative humidity is in the range 50-77%, chosen as representative scenarios for the analysis. It should be underlined that in between experiments, the test chamber was ventilated to remove the combustion products and provide fresh air. In case of not complete removal, the actual relative humidity in the chamber could have been altered with respect to the analysed range.

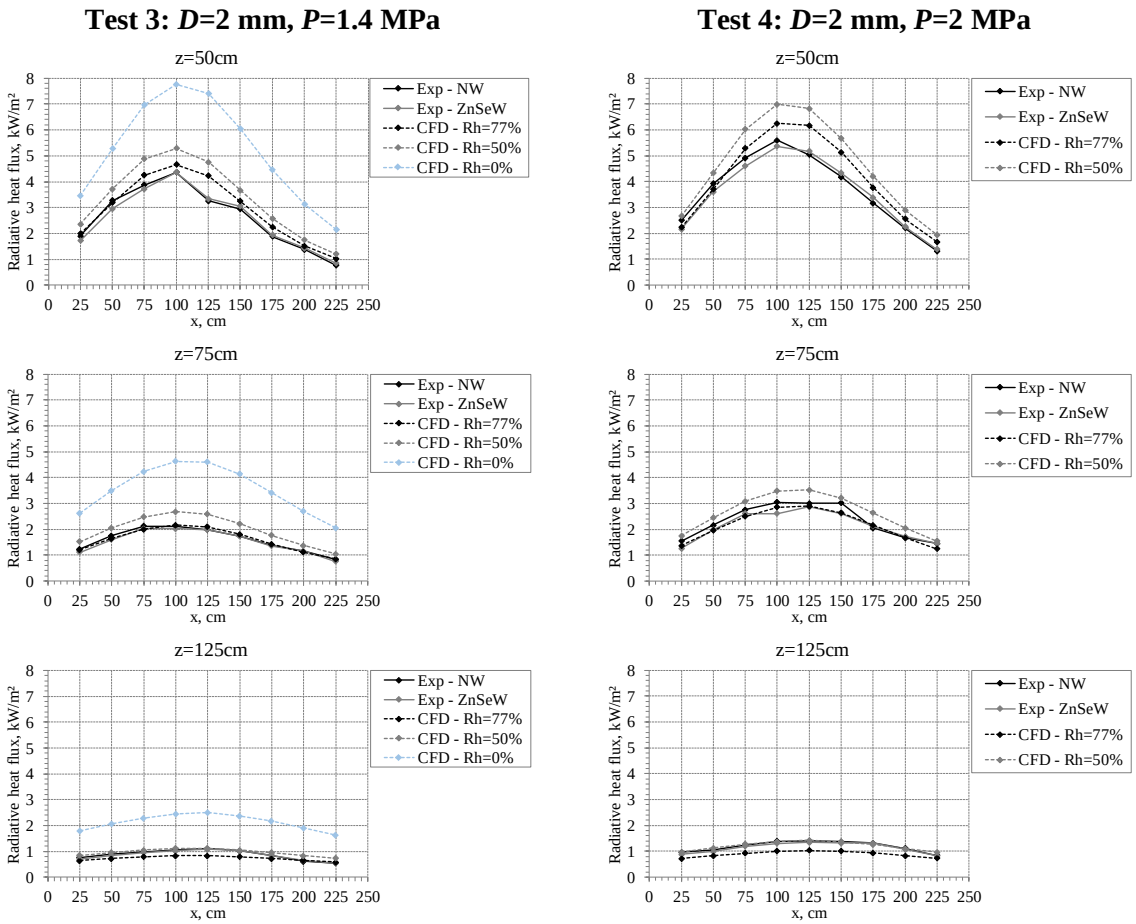


*Figure 7. Comparison of experimental and simulated radiative heat fluxes for Test 3 and Test 4.*

Simulations of Test 5 with Rh=77% well predict the experimental radiative heat flux for the ZnSeW sensors r1.1-r1.9 at 50 cm distance from the jet axis (see Fig. 8). At furthest distances, simulations underpredict experimental measurements, up to a relative variation of approximately 40% at z=125 cm. Simulations employing a relative humidity of 50% get closer to experiments (17% variation). Simulations of Tests 6 (Rh=77%) agrees well with experiment for the measurements at sensors r1.1-r1.4 located in the proximity of the first portion of the jet ($x$ up to 100 cm). Beyond this point, a significant variation is recorded, mainly oriented towards an underestimation of experimental measurements. This is consistent with the underprediction of flame length and thus the zone emitting radiation (see Table 4 below). Generally, it could be observed a worsening in predictive capability for larger release diameter (4 mm) when the relative humidity of 77% is considered. This may be associated to lower relative humidity in the chamber for these tests. Furthermore, it should be noted that the assumption of uniform sonic velocity at the nozzle, which may well approximate release conditions for smaller diameters ($D$=2 mm), may weaken for larger diameters ($D$=4mm). The effects would be seen on the spreading rate of the jet. Finally, it has been observed previously in simulations performed at HySAFER Centre on hydrogen releases from different nozzle shapes that the latter may affect the angle of the jet in the near field to the nozzle.

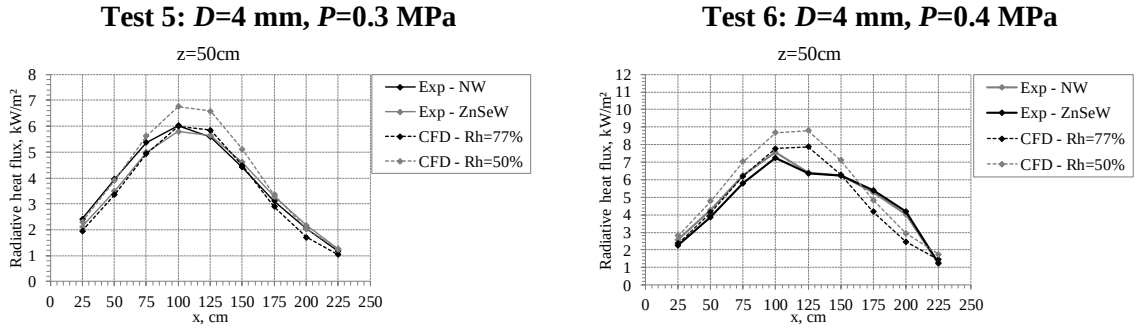

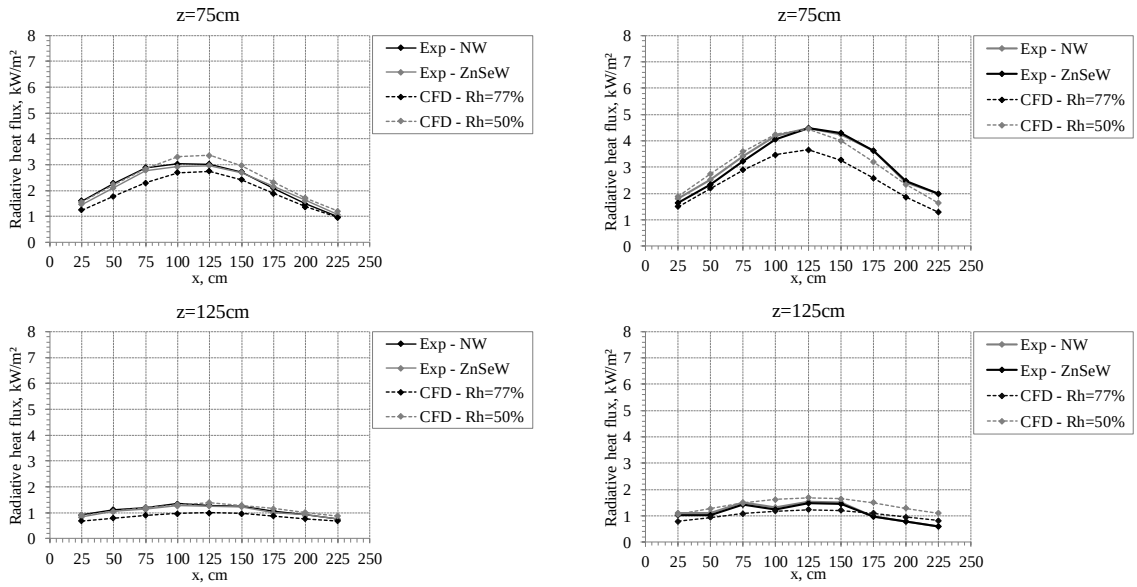


*Figure 8. Comparison of experimental and simulated radiative heat fluxes for Test 5 and Test 6.*

As widely discussed in the literature, an accurate estimation of flame length for hydrogen jet fires is not a trivial task, neither in experiments nor simulations. Thus, analysis of flame length shall be handled carefully and with the awareness about associated accuracy level. In simulations, a temperature region in the range 1300-1500 K was considered to correspond to the visible flame length [24]. Further criteria was the limit to OH mole fraction equal to 0.001 to indicate the most reacting zone based on work in [25]. Figure 6b reports the flame visualization according to the described criteria. It can be observed that the flame tip determined by OH mole fraction is located in between the 1300-1500 K region, thus, confirming that this range well represents the location of the combustion reaction zone. The flame is characterised by a tilted axis, due to buoyancy affecting the terminal portion of the jet. This somewhat differs from experimental observation statement that the flame is momentum-dominated. The authors believe that this may be due to the use of the notional nozzle in simulations, which models the jet as sonic with uniform velocity while the simulations of the near-field zone show a strong non-uniformity of the jet velocity immediately behind the Mach disk. This may cause a different velocity decay in the turbulent jet leading to an effect of buoyancy over momentum forces towards the tip of the flame and the deflection of the jet axis. This effect was experimentally observed in large scale jet fires [26]. Table 4 reports the experimental and simulated flame lengths. Flame length in simulations was calculated as the furthest $x$ coordinate along the tilting jet axis from the release where the criteria were met. Figure 6b shows that this point may not be on the original jet fire axis, i.e. the release direction, but located above it due to the flame axis tilt. Overall, simulations well predict the experimental flame length for Tests 3, 4 and 5. The largest difference, yet within acceptable 15%, was observed for Test 6. Furthermore, experiments showed that the decrease of storage temperature from 290 K to 80 K caused the flame length to increase from 1.25 m to 1.66 m for a same mass flow rate of 3.3 g/s. This is due to the higher density of combustible gas and the higher thermal expansion of combustion products for the cryogenic releases.

*Table 4. Comparison of experimental and simulated flame lengths.*

| **Test** | **3** | **4** | **5** | **6** |
|---|---|---|---|---|
| Experiment, m | 1.66 | 1.83 | 1.66 | 2.08 |
| CFD 1300 K, m | 1.68 | 1.89 | 1.72 | 1.86 |
| CFD 1500 K, m | 1.51 | 1.70 | 1.57 | 1.70 |
| CFD $mf_{OH} = 0.001$, m | 1.60 | 1.81 | 1.65 | 1.79 |

*4.3.1. Convergence and sensitivity of numerical simulations*

Simulations are steady-state type. A solution was considered converged when the axial distributions of temperature, $H_2O$ and OH mole fractions, velocity, and the radiative heat flux at the sensors did not

change with the advancement of iterations. Convergence was reached at 15,000 iterations and required about 20 hours to calculate on a 62 CPU machine.

A mesh sensitivity analysis was conducted on Test 3 (Rh=77%) to ensure grid independence of simulations. The CV size is halved at the nozzle, in the jet fire area and its surroundings up to the sensors. The refined grid has 4,372,060 CVs. Calculation time for 1,000 iterations raises from about 1.4 h to 5 h for the finer mesh. Relative maximum variation of radiative heat flux decreased from 8% for the sensors line at 50 cm from the jet axis to 4% at 75 cm, and to less than 2% at 125 cm. This may lead to the conclusion that sensitivity to the mesh of radiative heat flux results decreases with the distance/vicinity to the jet fire. A variation of 3% was recorded on the simulated flame length. Overall, these deviations are considered acceptable concluding that there is numerical grid convergence.

Study in [27] suggested that ground reflectance may have a significant effect on the near-field radiative heat flux measurements. The effect of ground emissivity was assessed for Test 6 by increasing it from 0.6 to 1, which means total absorption of incoming radiation. Radiative heat flux varied by 1% for the sensors located at 50 cm from the jet axis, and by 3% for those located at 75 cm. It is concluded that the ground emissivity has a negligible effect on the radiation recorded in the proximity of the jet fires. This conclusion may differ from observations in [27] because of the smaller jet fire scale compared to release in [27] (20.9 mm and 6 MPa), and the larger distance between the ground and the radiometers, which could be sufficient to absorb the reflected radiation by the water vapour in the air.

As described in Section 4.2, the lateral and top test chamber walls are defined as pressure outlets of the domain, i.e. open atmosphere, to prevent the accumulation of combustion products in an enclosed space for the applied steady-state simulations. A simulation is performed for Test 6 and Rh=50% by including the chamber walls at the sides of the domain with emissivity equal to 0.6 as per steel. A maximum variation of 3% in radiative heat flux is recorded for the sensors at 50 and 75 cm from the jet axis and about 5% for the sensors at 125 cm. This is considered to be negligible and the assumption of open boundaries on the sides of the jet fires does not undermine the predictive capability of the CFD model.

*4.3.2. Effect of air humidity*

As observed in Figs. 7 and 8, simulated radiative heat flux at sensors is sensitive to the assumed water vapour content in the air. Relative humidity in the environment may be highly variable throughout different locations and times of the year. Similar variations may be found as well between the outer (open atmosphere) and inner spaces, such as laboratories, etc. However, assumption of dry air in absence of exact experimental data on relative humidity may result in a significant overestimation of simulated radiative heat flux in the surroundings of a jet fire, due to the absence of absorption of energy by the water vapour in the air. A simulation of Test 3 is conducted to assess quantitively the effect of dry air assumption (Rh=0%). Figure 7 shows the resulting radiative heat flux and compares it to the radiation levels in case of relative humidity in the air of 77% and 50%. The absence of water vapour causes an increase of radiative heat flux recorded at 50 cm by approximately 1.7 times and up to 3 times at 125 cm distance compared to the case with Rh=77%. Values of radiative heat flux as high as 7.78 $kW/m^2$ are recorded at 50 cm distance from the jet axis and 2.52 $kW/m^2$ at 125 cm. The increase of air transmission coefficient with the decrease in relative humidity is ought to not be sufficient to justify the corresponding increase in radiative heat flux. In fact, it was seen that variation of relative humidity in simulations affects the distribution of properties and flame shape of the jet fire. Figure 9 presents the axial distribution of temperature along the release direction and along the radius at 1 m distance from the release point. As expected, simulation for dry air results in a slightly higher peak temperature. However, dry air assumption affects considerably the simulated extent of the high temperature zone, both parallel and perpendicular to the release direction as shown in Fig. 9. The tilted flame length defined by 1300K criteria increases from 1.68 to 1.76 m when relative humidity is varied from 77% to 0%. The absence of water vapour leads as well to a wider flame in radial direction to the jet, characterised by higher temperature and water vapour. As an example, flame width defined by 1300K criteria increases from 0.24 m to 0.32 m (see Fig. 9b) at 1 m from the release point. The larger volume of emitting water vapour at higher temperature (emitted radiation is proportional to the temperature to the power of 4) along with no attenuation from air in case of Rh=0% will be the cause of the increase of radiative heat flux at the sensors. Finally, it was seen that the absence of humidity in air doubles the amount of radiation reflected from the ground which may reach the radiometers. Overall, it can be

concluded that the CFD model is highly sensitive to humidity in air, and simulations using a dry air assumption may be far from reality leading to significant overestimations of radiation and flame length.

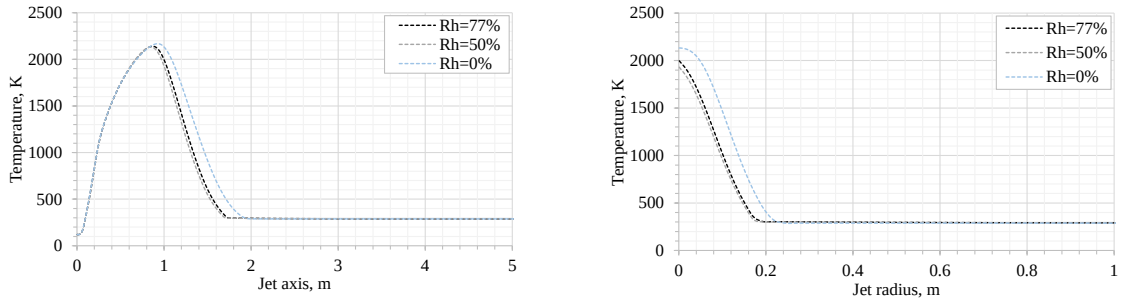


*Figure 9. Effect of air humidity on jet fire temperature along the axis (a) and along the radius at 1 m from the release point (b).*

### *4.3.3. Hazard distances for cryogenic horizontal jet fires*

The jet flame emits radiation and influences temperature distribution in its surroundings, producing hot air currents harmful to people. The experimental data on temperature distribution along a hydrogen jet flame trajectory measured in [10, 28, 29] were analysed in [6]. The study [6] correlated the temperature distribution as a function of the distance from the release point normalised by the flame length, to derive the following hazard distances using published harm criteria for people:

- "No-harm" hazard distance (70°C for any exposure duration): $x$=3.5$L_f$;
- "Pain" hazard distance (115°C for 5 minutes exposure): $x$ =3$L_f$;
- "Fatality" hazard distance (309°C, third-degree burns for 20 s exposure): $x$ =2$L_f$.

Temperature distributions analysed in [6] and associated hazard distances are referred to either vertical jet flames or to momentum-dominated horizontal jet fires and generated combustion products. Temperature distribution and associated hazard distances along the release direction may change for horizontal jet fires because of combustion products' buoyancy. The CFD model showed to well represent radiative and flame length characteristics, hence, it is presumed that it well represented the distribution of hot combustion products too. Figure 10 shows the calculated temperature along the release direction at a height of 0.9 m, i.e. the height of the release. Distribution is reported as a function of the distance normalised to the flame length calculated according to the temperature criterion (1300-1500 K). The temperature distribution for the jet fire experiments and simulated cryogenic horizontal jet fires is similar within the jet fire for distances lower than $x$=0.6 ÷ 0.7$L_f$. Beyond this distance, temperature rapidly decreases along this horizontal line reaching ambient temperature already within $x$=1.2$L_f$. Indeed, the effect of buoyancy was seen already towards the tip of the flame, causing a rapid rise of hot combustion products. Considering the flame length calculated by 1500 K limit, maximum distances to the harm thresholds are seen to decrease as follows along the release direction at height 90 cm: "fatality" distance at $x$=1$L_f$; "pain" limit at $x$=1.1$L_f$; "no harm" limit at $x$=1.15$L_f$.

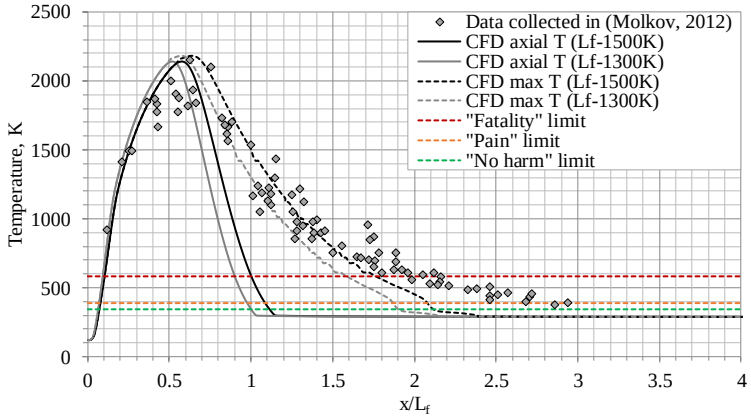


*Figure 10. Temperature as a function of distance normalised to flame length ($L_f$) for jet fires experiments* [6] *(diamonds) and horizontal jet fire in CFD simulation of Test 3 (P=1.4 MPa, D=2 mm): temperature distribution*

*along the horizontal release direction at height 90 cm (solid curves) and maximum temperature calculated across the entire domain height at a given distance x (dashed curves).*

However, the maximum temperature at a certain distance from the release point may not be located on the release direction due to the effect of buoyancy on combustion products (see Fig. 6a). Thus, a second analysis is performed to retrieve the maximum temperature recorded at any height $y$ up to 3.4 m for a certain distance $x$. Matlab software was used to process simulations results in all the CVs (>1million) in the domain. Figure 10 (dashed curves) shows the retrieved maximum temperature as a function of the distance $x$ normalised by the flame length for distances approximately $x$>0.5$L_f$, beyond which point buoyancy started to cause tilting of the jet fire axis. Temperature distributions for the simulated horizontal and experimental jet fires show similar trend up to $x$=1.5$L_f$. Beyond this point, it can be observed that the simulated cryogenic horizontal jet fire shows a faster decrease in the maximum temperature with the distance $x$ from the release. The criterion of 1500 K for the flame length in CFD simulations is considered in the following statements. The hazard distances according to harmful temperature criteria can be calculated as follows: "fatality" limit at $x$=1.75$L_f$; "pain" limit at $x$=2.1$L_f$; "no-harm" limit at $x$=2.2$L_f$. The latter normalised distance corresponds to 3.3 m from the release point. Ambient temperature is reached at the horizontal distance $x$=2.3$L_f$. Similar results are obtained for the remaining three tests, with exception of Test 6 where distance is slightly reduced to $x$=2.0$L_f$ for a "no-harm" limit. Thus, it may be concluded that hazard distances for hot air currents as defined for vertical or momentum-dominated horizontal jet fires may be too conservative if applied to the cryogenic horizontal jet fires under investigation. It should be highlighted that these distances and change of multiplier are referred to the open space scenario and only to the particular tests investigated.

It has been observed that the horizontal direction of a jet leads to a significant decrease in "no-harm" hazard distance from a jet fire due to buoyancy of combustion products. However, it is fundamental to know if longer distances should be ensured to avoid harm by thermal radiation of the jet fire in its surroundings. Exposure to the radiative heat flux of a jet fire can have different hazard distances based on harm levels: first, second or third-degree burns. The potential damage depends on the vulnerability of the target, which is determined by age, health conditions, etc. The following harm criteria [3] are used to assess the hazard distances from jet fire by thermal radiation:

- "100% lethality" in 1 min: 25.0 kW/m$^2$.
- "Second-degree burn" after 20 s: 9.5 kW/m$^2$.
- "First-degree burn": 4.0 kW/m$^2$.
- "No-harm" for long exposures: 1.6 kW/m$^2$.

Simulations with a relative humidity equal to 77% are considered, as more representative of the open atmosphere conditions. Results analyse the incident radiation in each control volume, which does not take into account the incident ray angle on a surface. This provides a conservative estimate. Table 5 reports the results obtained for all the four tests simulated in the study. The zones designed by limits for "100% lethality" in 1 minute (25.0 kW/m$^2$) and "second degree burns" after 20 seconds (9.5 kW/m$^2$) follow the distribution of the flame and combustion products (see Fig. 6). It is expected that in these areas along the tilting flame axis, the convective and conductive heat flux associated with the high temperature combustion products and hot currents overcomes the radiative heat flux. On the other hand, simulation results showed that the "no-harm" by the radiation limit of 1.6 kW/m$^2$ and the "first-degree burn" limit (4.0 kW/m$^2$) are reached at the indicated axial distance regardless of the height of the target, whereas it was seen that temperature along the release direction would decay to "no-harm" level within $x$=1.15$L_f$ (1.75 m). Therefore, Table 5 reports only the hazard distances along the release direction associated to "no-harm" and "first-degree burn" criteria. Considering results for Test 3, it can be observed that the axial "no-harm" distance is equal to 4.75 m ($x$=3. 2$L_f$). This hazard distance is larger to that obtained along the tilting flame axis for the no-harm criterion by the temperature of hot gases (3.3 m), which corresponds to $x$=2.2$L_f$. "No-harm" axial distances consistent with Test 3 are obtained for the remaining three tests (x=3.0-3. 2$L_f$). The "no-harm" distance on the sides of the jet fire reaches the domain boundaries (2.7m) for all the four tests, preventing a throughout analysis and comparison.

*Table 5. Hazard distances by thermal radiation from the jet fire perpendicularly to the direction of the release (radial) and along the release direction (axial). Validity domain: P=0.3-2.0 MPa, T=80 K, D=2-4 mm.*

| Harm level | "100% lethality" in 1 min: 25.0 kW/m$^2$ | "Second-degree burn" after 20 s: 9.5 kW/m$^2$ | "First-degree burn": 4.0 kW/m$^2$ | | "No-harm" for long exposures: 1.6 kW/m$^2$ | |
|---|---|---|---|---|---|---|
| Direction | Radial | Radial | Radial | Axial | Radial | Axial |
| Test 3 | 0.31 | 0.48 | 0.90 | 3.19 | 2.70* | 4.75 |
| Test 4 | 0.39 | 0.60 | 0.94 | 3.42 | 2.70* | 5.26 |
| Test 5 | 0.29 | 0.52 | 0.82 | 3.11 | 2.70* | 4.77 |
| Test 6 | 0.32 | 0.57 | 0.84 | 3.06 | 2.70* | 5.10 |

Note: * - 2.70 m is the distance where the domain boundary is located.

Overall, it can be concluded that for the horizontal jet fires under investigation the distances along the jet axis associated to the thermal radiation "no-harm" criterion resulted to be longer than hazard distances calculated by "no-harm" criterion by temperature. The CFD model is showed to be an accurate tool to predict thermal radiation from a hydrogen jet fire. The results of this numerical CFD study should be harmonised with the development of a reduced tool for the assessment of thermal hazards from horizontal jet fires in an accurate and faster way. To the authors' knowledge, no such widely validated tool is available in the peer-reviewed literature. Further research should be performed in this direction.

A final analysis addresses the calculation of hazard distances through evaluation of the thermal dose. The assessment is conducted on the sides of the jet fire, as it is expected that in this zone thermal radiative heat flux will be dominant to the convective and conductive heat fluxes associated to the high-temperature combustion products. The thermal dose is a comprehensive parameter calculating the level of harm as a function of the exposure duration ($t$, s) in addition to the incident thermal radiation ($I$, kW/m$^2$). It is expressed in terms of thermal dose (TD) measured in [(kW/m$^2$)$^{4/3}$s]:

$$TD = \int_0^t I(t)^{4/3} dt \,. \tag{1}$$

Thermal dose harm levels for infrared radiation are considered [3] being more conservative and indicated for water vapour emitted thermal radiation [30]. A thermal dose range of 870-2640 (kW/m$^2$)$^{4/3}$s is indicated for third-degree burns and 240-730 (kW/m$^2$)$^{4/3}$s for second-degree burns. A threshold range of 80-130 (kW/m$^2$)$^{4/3}$s is indicated for first-degree burns. Given values are for people not wearing protecting clothes. The thermal dose assessment is used to get more insights into the exposure time leading to harm from thermal radiation. Table 5 showed that a person located at 0.31 m from the jet axis would incur into "100% lethality", i.e. 78-100% of burned body area [10], if exposed to 25 kW/m$^2$ for 1 minute to the jet fire in Test 3. This corresponds to TD=4386 (kW/m$^2$)$^{4/3}$s, which is well beyond the thermal dose range for third-degree burns. Results from thermal dose analysis suggests that the exposure time to 25 kW/m$^2$ shall be below 25 seconds to not incur into third-degree burns (TD=870 (kW/m$^2$)$^{4/3}$s). At 0.48 m from the jet fire, second-degree burns are expected after 20 s exposure to 9.5 kW/m$^2$ (TD=402 (kW/m$^2$)$^{4/3}$s). Thermal dose calculation suggests that exposure should be less than 17 s to prevent occurring of second-degree burns. If the exposure time is prolonged to about 60 s, third-degree burns would occur. Finally, thermal dose calculation at 0.90 m from the jet suggests that the exposure time to a radiation level of 4.0 kW/m$^2$ should be minor than 17 s to not incur into first-degree burns. An exposure time prolonged to approximately 60 s would lead to second-degree burns.

The thermal dose is a valuable tool to assess the feasibility of short-term activities and emergency operations, such as opening or closing valves, rescue operations, etc. It is unlikely, as well as advised against it, that emergency personnel will approach from downstream the jet flame. Conversely, an approach to the scene from the hydrogen jet fire sides is generally suggested and applied. Thus, the analysis of thermal dose for first responders is conducted only aside the jet flame. Facility operators or emergency personnel wearing standard workwear are characterised by similar tolerance to radiative heat flux of people not wearing protecting clothes [31]. Thus, distances and exposure time identified above maintain their validity. Firefighters responding to a fire will wear thermal protective clothing, increasing the tolerable levels of radiative heat flux. Authors of study [31] indicated that 168 s is the tolerance time for pain for a standing firefighter exposed to heat fluxes up to 4.6 kW/m$^2$. The simulation

results show that for Test 3 firefighters can stay as close as 0.71 m from the jet axis to not incur into pain, receiving a thermal dose of approximately 1285 $(kW/m^2)^{4/3}s$. A limit of 6.3 $kW/m^2$ is given for an operating time of 5 minutes if firefighters are wearing aluminised clothing (TD≈3490 $(kW/m^2)^{4/3}s$), reducing further the distance from the jet axis to about 0.59 m.
It should be noted that conclusions on the hazard distances analysis are valid only for the jet fires under investigation with storage pressure in the range 0.3-2.0 MPa, storage temperature of 80 K and release diameter in the range 2-4 mm.

## 5. Conclusions

The ***originality*** of this study includes the investigation of the effect of conjugate heat transfer through a pipe wall on the flow of cryogenic hydrogen and ultimately on the thermal hazards from the resulting jet fires using the validated CFD model. The under-expanded jet theory without pressure losses and heat transfer was found to reproduce experimentally measured mass flow rate with an accuracy of ±15% for releases at ambient temperature. However, the approach was found to be not accurate for cryogenic releases, leading to an overestimation of calculated mass flow rate up to 37% for the test with release pressure and temperature equal to 2 MPa and 80 K respectively (Test 4). The use of discharge coefficient to match experimental mass flow rate was not capable to represent cryogenic releases, as it does not account for heat transfer in the release system and thus corresponding change of temperature and pressure in the flow.

The heat transfer was assumed to cause an increase of temperature from 67 K to 98-127 K at the real nozzle exit depending on the storage pressure and nozzle diameter. A parametric study was conducted to estimate the inlet temperature in the simulated release pipe leading to the same mass flow rate as in experiments. Calculated hydrogen parameters at the real nozzle exit were implemented to define parameters at the notional nozzle exit used as the boundary conditions for the hydrogen release source in CFD simulations of jet fires. The CFD model previously validated for vertical hydrogen jet fires with release pressure up to 0.5 MPa and temperature in the range 48-82 K was employed. A modification to the calculation procedure was proposed to accelerate the steady-state simulations by updating chemistry and radiation parameters model every 5 and 200 flow iterations respectively. Calculation time was reduced by a factor of 3 with a maximum 2% variation on measured radiative heat flux.

The ***rigour*** of this study is in further validation of the CFD model against four unique experiments on cryogenic hydrogen horizontal jet fires with release pressure increased up to 2 MPa and temperature equal to 80 K. The CFD model validation domain was expanded to cryogenic jet fires with higher release pressure and horizontal direction of the jet. Furthermore, a parametric study on the effect of numerical and experimental parameters on the sensitivity of simulation results to them was conducted. Overall, the trend of radiative heat flux distribution aside the jet axis was well reproduced by simulations. Tests with release diameter equal to 2 mm (pressure up to 2 MPa) and 4 mm (pressure equal to 0.3 MPa) were well reproduced by the simulations. Prediction accuracy is within 10% for the test at cryogenic storage pressure 1.4 MPa, with exception of few sensors located close to the jet axis. Accuracy for the test with pressure 2 MPa is within 20%. In both tests, the experimental radiative heat flux was somewhat underestimated at the furthest distance from the jet axis (125 cm). Predictive capability for the test with nozzle diameter 4 mm and storage pressure 0.4 MPa improved when a relative humidity equal to 50% was employed. Overall, the experimentally measured flame length was predicted by simulations with very good accuracy within ± 15%.

Simulations results were found to have great sensitivity to presence of water vapour content in air, which affected not only the attenuation of thermal radiation but as well the flame shape and extent. Variation of ground emissivity and inclusion of steel emitting walls in the domain had a negligible effect on the radiative heat flux recorded at the sensor locations.

The ***significance*** of the work is given by the provision of a contemporary validated CFD tool to assess thermal hazards from cryogenic jet fires and avoid over-conservative hazard distances. It concluded that engineering correlations available in the literature to predict hazard distances according to harmful temperatures may not be suited for the horizontal hydrogen jet fires. The buoyancy of combustion products has a positive effect on the reduction of the "no harm" distance from $x$=3.5$L_f$ as presented in literature for vertical or fully momentum dominated horizontal jet fires, to $x$=2.2$L_f$ for the cryogenic

hydrogen horizontal jet fires under investigation. Thermal radiation leads to longer "no-harm" distances in the direction of the jet ($x$=3.0-3.$2L_f$) compared to hazard distance defined by temperature. Harmful distances on the side of the investigated experimental jets were calculated to be longer than the domain size, i.e. 2.7 m in the radial direction to the jet. Conclusions and change of multiplier between vertical and horizontal jet fire are valid for the particular tests investigated. The analysis of hazard distances was completed by the assessment of the thermal dose on the sides of the jet fire. The simulations showed that firefighters can stand without harm as close as 0.71 m to a jet fire axis for a time not exceeding 168 s. Overall, it is concluded that a throughout assessment of thermal hazards and associated distances from a hydrogen jet fire should combine the analysis of temperature, thermal radiation and thermal dose, as these were found to be complementary to each other.

## Acknowledgements

This research has received funding from the Fuel Cells and Hydrogen 2 Joint Undertaking (now Clean Hydrogen Partnership) under grant agreement No.779613 (PRESLHY), No.736648 (NET-Tools), No.826193 (HyTunnel-CS) and No.875089 (HyResponder). This Joint Undertaking receives support from the European Union's Horizon 2020 research and innovation programme, Hydrogen Europe and Hydrogen Europe research. The authors would like to acknowledge Innovate UK for funding the project "Northern Ireland Green Seas" (ID: 397841).

## References

[1] DOE. Technical Assessment: Cryo-Compressed Hydrogen Storage for Vehicular Applications. 2006.

[2] Friedrich A, Breitung W, Stern G, Veser A, Kuznetsov M, Fast G, et al. Ignition and heat radiation of cryogenic hydrogen jets. Int J Hydrogen Energy 2012;37:17589–98. https://doi.org/10.1016/j.ijhydene.2012.07.070.

[3] Lachance J, Tchouvelev A, Engebo A. Development of uniform harm criteria for use in quantitative risk analysis of the hydrogen infrastructure. Int J Hydrogen Energy 2011;36:2381–8. https://doi.org/10.1016/j.ijhydene.2010.03.139.

[4] Panda PP, Hecht ES. Ignition and flame characteristics of cryogenic hydrogen releases. Int J Hydrogen Energy 2017;42:775–85. https://doi.org/10.1016/j.ijhydene.2016.08.051.

[5] Cirrone D, Makarov D, Molkov V. Thermal radiation from cryogenic hydrogen jet fires. Int J Hydrogen Energy 2019;44:8874–85. https://doi.org/10.1016/j.ijhydene.2018.08.107.

[6] Molkov V. Fundamentals of Hydrogen Safety Engineering I Download free books at Vladimir Molkov Fundamentals of Hydrogen Safety Engineering I. 2012.

[7] Hall JE, Hooker P, Willoughby D. Ignited releases of liquid hydrogen: Safety considerations of thermal and overpressure effects. Int J Hydrogen Energy 2014;39:20547–53. https://doi.org/10.1016/j.ijhydene.2014.05.141.

[8] Cirrone D, Makarov D, Molkov V. Near Field Thermal Dose of Cryogenic Hydrogen Jet Fires. Ninth Int. Semin. Fire Explos. Hazards, 2019, p. 1360–6.

[9] Breitung W, Stern G, Veser A, Friedrich A, Kutznetsov M, Fast G, et al. Final Report:Experimental and theoretical investigations of sonic hydrogen discharge and jet flames from small breaks. 2009.

[10] LaChance JL. Progress in risk assessment methodologies for emerging hydrogen applications. Sixth Int. Short Course Adv. Res. Work. "Progress Hydrog. Saf. – Regul. codes Stand., Belfast, Northern Ireland, UK: 2010.

[11] Molkov V, Makarov V, Bragin M V. Physics and modelling of underexpanded jets and hydrogen dispersion in atmosphere. Phys Extrem States Matter 2009:146–9.

[12] Cirrone D, Makarov D, Molkov V. Cryogenic hydrogen jets: flammable envelope size and hazard distances for jet fire. ID191. Int. Conf. Hydrog. Saf., Adelaide, Australia: 2019.

[13] Smagorinsky J. General circulation experiments with the primitive equations. I. The basic experiment. Mon Weather Rev 1963;3:99–164.

[14] Bell IH, Wronski J, Quoilin S, Lemort V. Pure and Pseudo-pure Fluid Thermophysical Property Evaluation and the Open-Source Thermophysical Property Library CoolProp. Ind Eng Chem Res 2014;53:2498–508.

[15] Taira Y, Saburi T, Kubota S, Sugiyama Y, Matsuo A. Numerical investigation of hydrogen leakage from a high pressure tank and its explosion. Int. Conf. Hydrog. Saf., Yokohama, Japan: 2015, p. 1–11.
[16] Properties of materials n.d. http://www.caffnib.co.uk/properties.html (accessed September 30, 2020).
[17] Shih TH, Liou WW, Yang A, Shabbir Z. A new eddy-viscosity model for high Reynolds number turbulent flows—model development and validation. Comput Fluids 1995;24:227–238.
[18] Magnussen B. On the structure of turbulence and a generalized eddy dissipation concept for chemical reaction in turbulent flow. Am Inst Aeronaut Astronaut 1981.
[19] Molkov V, Shentsov V, Brennan S, Makarov D. Hydrogen non-premixed combustion in enclosure with one vent and sustained release: Numerical experiments. Int J Hydrog Energy 2014;39:10788–10801.
[20] Murthy JY, Mathur SR. A finite volume method for radiative heat transfer using unstructured meshes. 36th AIAA Aerosp Sci Meet Exhib 1998;M. https://doi.org/10.2514/6.1998-860.
[21] Hubbard C., Tien GL. Infrared Mean Absorption Coefficients of Luminous Flames and Smoke. J Heat Transf 1978;100:235–239.
[22] Omega. Emissivity of common materials n.d. www.omega.com/literature/transactions/volume1/emissivitya.htm (accessed February 15, 2017).
[23] Weather&Climate. Average Humidity In Karlsruhe (Baden-Württemberg) 2020. https://weather-and-climate.com/average-monthly-Humidity-perc,karlsruhe,Germany (accessed October 15, 2020).
[24] Schefer R, Houf B, Bourne B, Colton J. Experimental Measurements to Characterize the Thermal and Radiation Properties of an Open-flame Hydrogen Plume. Proc 15th Annu Hydrog Conf Hydrog Expo, 2004.
[25] Yates D. Innovative solutions to reduce separation distances in on-board hydrogen storage. PhD Thesis. 2016.
[26] Ekoto IW, Ruggles AJ, Creitz LW, Li JX. Updated jet flame radiation modeling with buoyancy corrections. Int J Hydrogen Energy 2014;39:20570–7. https://doi.org/10.1016/j.ijhydene.2014.03.235.
[27] Wang CJ, Wen JX, Chen ZB, Dembele S. Predicting radiative characteristics of hydrogen and hydrogen/methane jet fires using FireFOAM. Int J Hydrogen Energy 2014;39:20560–9. https://doi.org/10.1016/j.ijhydene.2014.04.062.
[28] Barlow RS, Carter CD. Relationship among nitric oxide, temperature and mixture fraction in hydrogen jet flames. Combust Flame 1996;104:288–99.
[29] Imamura T, Hamada S, Mogi T, Wada Y, Horiguchi S, Miyake A, et al. Experimental investigation on the thermal properties of hydrogen jet flame and hot currents in the downstream region. Int J Hydrogen Energy 2008;33:3426–35. https://doi.org/10.1016/j.ijhydene.2008.03.063.
[30] Howell JR, Mengüc MP, Siegel R. Thermal Radiation Heat Transfer. 6th Editio. Taylor and Francis Group; 2016.
[31] Heus R, Denhartog EA. Maximum allowable exposure to different heat radiation levels in three types of heat protective clothing. Ind Health 2017;55:529–36. https://doi.org/10.2486/indhealth.2017-0137.